Int. J. Electrochem. Sci., 14 **(2019)** 4240 – 4253, doi: 10.20964/2019.05.13

International Journal of
ELECTROCHEMICAL
SCIENCE
www.electrochemsci.org

Enhancement of the Anti-Corrosion Performance of Composite Epoxy Coatings in Presence of BTA-loaded Copper-Based Metal-Organic Frameworks

Di Yin[1,2,3], *Zongxue Yu*[1,2,3,*], *Legang Chen*[1,2,3], *Kunyao Cao*[1,2,3]

[1] Southwest Petroleum University, School of Chemistry and Chemical Engineering, Chengdu, 610500, China;
[2] Oil & Gas Field Applied Chemistry Key Laboratory of Sichuan Province, Southwest Petroleum University, Chengdu, Sichuan 610500, PR China;
[3] State Key Laboratory of Oil & Gas Reservoir Geology and Exploitation, Southwest Petroleum University, Chengdu, Sichuan 610500, PR China
[*]E-mail: haiqingy@163.com

Received: 8 November 2018 / *Accepted:* 6 January 2019 / *Published:* 10 April 2019

This study reports a new strategy for enhancing anti-corrosion properties of epoxy coatings. For this purpose, copper-based metal-organic frameworks (Cu-MOF) were applied as hosts of corrosion inhibitor (benzotriazole, BTA). The BTA-Cu-MOF was characterized using Infrared spectroscopy (FTIR), Thermogravimetric analysis (TG) and X-ray diffraction (XRD). Furthermore, the BTA loading in MOFs was determined by UV-vis and TGA. And MOFs were well dispersed in epoxy resin which was confirmed by SEM and XRD. Compared to the pure epoxy coatings, epoxy coating including BTA-Cu-MOF had greater radius of impedance arc via the electrochemical impedance spectroscopy (EIS) and higher water contact angle, which revealed the samples enhanced corrosion resistance of pure epoxy coatings. At the same time, the corrosion protection performance of epoxy coating with 2 wt% BTA-Cu-MOF were preferable than other coatings.

Keywords: copper-based metal-organic frameworks (Cu-MOF), benzotriazole, epoxy coating, corrosion resistance

1. INTRODUCTION

Metal, one of the most common materials, is employed in industry and daily life. However, corrosion of metal is a serious worldwide problem that gives rise to in great economic losses, the material failure, reduction in efficiency and serious environmental problems. Several methods such as organic coatings, corrosion inhibitors or hybrid protective coatings have successfully been introduced

in order to control or mitigate corrosion processes that take place on the steel surface [1-4]. The epoxy coating (one of organic coatings) is utilized for protecting metal structures against corrosion through providing a physical barrier between the corrosive environment and the metal surface [5-8]. Nonetheless, the epoxy coating is one of the thermosetting coatings and it can release some volatiles (solvent, water and curing products) during the process of curing, which cause a large deal of microphones and cracks [9-11]. Therefore, some corrosion medium such as Cl^-, H_2O and H^+ can penetrate into the interface of coating/metal through the tiny holes or crack, which decrease the anticorrosion of protective layer.

To solve this problem, researchers have proposed an effective and simple method that adding the BTA (benzotriazole) into epoxy coatings to resist the corrosive of metal, which is due to that the BTA is an environmental friendly, cost effective and excellent corrosion inhibitor[12, 13]. However, if the BTA is firsthand added into epoxy coatings, BTA will cause more micropores in the epoxy coating[14]. Therefore, recent researches [15-17] showed that encapsulation of corrosion inhibitors into micro-or nanocontainers is a prospective method for coating. The coating is called intelligent coating or smart coating and it not only provides a barrier to inhibit the corrosion of metal, but also increases an “active” protection mechanism[18-22]. For example, Suna and coworkers reported that benzotriazole (BTA) loaded HNT were added to a silicate-based electrolyte to produce PEO coatings on AM50 alloy. The BTA-HNT enhanced corrosion resistance due to a self-healing effect[23].

Metal organic frameworks (MOFs) are the new class of nanoporous materials, have recently received significant attention. MOFs materials have extraordinary permanent porosity, large pore volume and low density with high surface area for a wide range of applications including gas storage or separation, catalysis, drug delivery and imaging[24, 25]. Specifically, drug delivery [26-29] was similar to “smart” coatings. Their working principle was that the material (drug or corrosion inhibitor) was released from the hosts such as MOFs, nanometer materials with cavity when the environmental change or a particular circumstance. Therefore, the MOFs are an excellent material to load the corrosion inhibitor. Meanwhile, the MOFs are well established in the field of electrochemistry, materials for rechargeable BTAteries, super capacitors, fuel cells, and electrocatalysis or corrosion inhibition [30-33].

In this paper, the copper-based metal-organic frameworks (Cu-MOF), as corrosion inhibitor (BTA) hosts, were inserted in the epoxy resin to prepare the smart coatings. The release of BTA was under magnetic stirring at a constant rotational speed and identified by UV-vis and TGA. The BTA-Cu-MOF was equably dispersed in the epoxy coating. The BTA-Cu-MOF was determined to improve the anticorrosion performance of epoxy coatings in 3.5 wt% NaCl solution. And the optimum weight of BTA-Cu-MOF was 2 wt%.

2. EXPERIMENTAL

2.1. Materials

The $Cucl_2{\cdot}2H_2O$, BTA (benzotriazole), DMF (N, N-Dimethylformamide), EtOH, trimesic acid, triethylamine and CH_2Cl_2 were provided by Kelong Chemical Co. Ltd., Chengdu, China. The epoxy

emulsion (WSP-6101) and its hardener were supplied by Bluestar technology wuxi resin factory. Deionized water was produced by water purification machine (UPCIII-40L, Ulupure).

2.2. The preparation of Cu-MOF and BTA-Cu-MOF

Trimesic acid (1.5 g) and $Cucl_2 \cdot 2H_2O$ (2.2 g) were dissolved in 72 ml of 1:1:1 ratio of DMF/EtOH/H_2O mixture. Under stirring condition, triethylamine was added drop wise until the PH=7.00 and the reaction mixture were stirred for 24 h. The precipitate was centrifuged and washed by DMF. And then the suspension was immersed in 50 ml of CH_2Cl_2 overnight. The next day, the precipitate was again immersed in CH_2Cl_2 overnight. The resulting blue suspension was centrifuged and washed by the DMF and EtOH to remove the impurities and unreacted materials. Finally, the blue Cu-MOF was prepared by drying above blue suspension[34].

0.2g Cu-MOF was uniformly dispersed in the 50 ml EtOH solution (containing 2g BTA). After 24h under stirring condition, the precipitates were filtered out and washed by EtOH repeatedly to remove excessive BTA. In this way, the BTA-Cu-MOF was obtained.

2.3. Preparation of BTA-Cu-MOF/EP coating

The BTA-Cu-MOF/EP coating was prepared by adding BTA-Cu-MOF (1 wt%, 2 wt%, 3 wt% and 5 wt%) and Cu-MOF (2 wt%) into the epoxy resin, and spraying above epoxy paint on the cleanly surface of steel sheet (10mm × 10 mm×1mm), and then solidifying the mixture at 60 °C for 1 h and at 120 °C for 1h, and at 180 °C for 1.5 h and at 220 °C for 0.5 h.

2.4. Characterization

The surface morphology and microstructures of the as-prepared samples were observed through scanning electron microscopy (SEM; JSM-7500F, JEOL, Tokyo, Japan). Fourier transform infrared (FTIR) spectra of the as-prepared samples were obtained from WQF-520 at wave number range 4000–400 cm^{-1}. X-ray diffraction (XRD) analysis was conducted on a PANalytical with a Cu Kα radiation source at a scan rate of 2° min^{-1} ranging from 5° to 70° (2θ). Thermogravimetric analysis (TGA; STA449F3) was performed from 40 to 400 °C with a linear heating rate of 10 °C min^{-1} under nitrogen atmosphere.

To understand the release rate of BTA from the Cu-MOF, UV-vis spectroscopy was utilized. The UV-vis diffuse reflectance spectra of the as-prepared samples were measured on PerkinElmer Lambda 850UV-vis-NIR spectrometer, using BaSO4 as reference. The concentration-absorbance curve of BTA is obtained by measuring the absorbance of different concentration BTA/EtOH at 259nm (characteristic absorbance of BTA). The release experiments were performed in ethanol at room temperature. The suspension (50 ml) containing the BTA-Cu-MOF (0.05g) was constantly stirred in a conical flask. In order to set up equilibrium conditions, continuous magnetic stirring was used during the release process. The BTA can gradually release from the Cu-MOF with increasing time and the

concentration of BTA in the suspension was determined by the absorbance using UV-vis spectroscopy at 259 nm wavelengths. Meanwhile, it was also used to confirm whether BTA had been loaded in the Cu-MOF.

The corrosion resistance coatings was tested by an electrochemical workstation (EIS, CHI604D, China) in 3.5 wt% NaCl solution. These analyses were carried out at room temperature in a three-electrode cell including a saturated calomel electrode (reference electrode), platinum plate electrode (counter electrode) and steel substrates without and with treatments (working electrode with an area of 1 cm^2). Measurements were performed at a stable open circuit potential (OCP) in the frequency range of 10^5 to 10^{-2} Hz and at amplitude sinusoidal voltage of ± 10 mV. Also, potentiodynamic measurements were started from the cathodic direction (-250 mV) to the anodic direction (+250 mV) around OCP with 1 mV/s scan rate. EIS measurements were performed at different immersion times. The impedance data were analyzed and fitted using "ZSimpWin" software.

3. RESULTS AND DISCUSSION

3.1. The characterization of Cu-MOF material

Fig. 1 was the FT-IR curve of $CuCl_2 \cdot 2H_2O$, Cu-MOF, BTA-Cu-MOF. From the FT-IR curve of $CuCl_2 \cdot 2H_2O$, 1613 cm^{-1} and 3512 cm^{-1} were the characteristic peaks. The peak at 3455 cm^{-1} stretching vibration of the coordinated water molecules and a sharp bend vibration in 1638 cm^{-1} confirmed the presence of water in the Cu-MOF. The asymmetric and symmetric stretching vibrations of carboxylate group in the trimesic acid were observed at 1446 and 1375 cm^{-1} respectively. The aromatic (C–H) bending mode appeared at around 1101 cm^{-1}. Particularly, the all peaks of BTA-Cu-MOF are similar to Cu-MOF. Therefore, the Cu-MOF was successfully prepared.

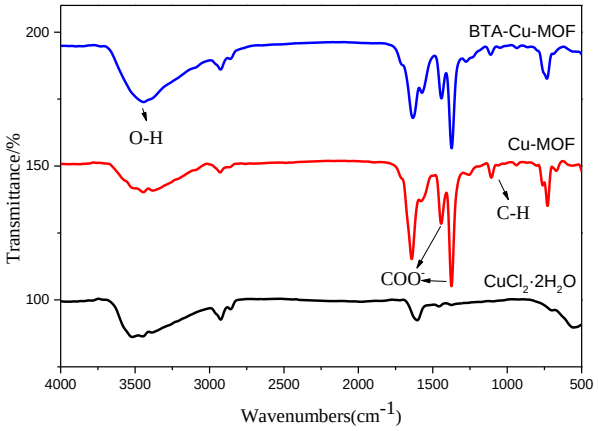

Figure 1. the FT-IR curve of $CuCl_2 \cdot 2H_2O$, Cu-MOF and BTA-Cu-MOF

The XRD patterns (Fig. 2) displayed diffraction peaks of BTA-Cu-MOF, Cu-MOF, $Cucl_2 \cdot 2H_2O$. The characteristic diffraction peak of $Cucl_2 \cdot 2H_2O$ were at 2θ=16.7° and 34.5°. And

characteristic diffraction peaks at 2θ= 9.6°, 13.6°, 14.8°, 15.2°, 16.6°, 17.6°, 19.2°, 20.4°, 2 4.3°, 26.1°, 29.5°, 35.3°, 39.3°, 41.6° and 47.3° were assigned to Cu-MOF in accord with the literature [34]. Compared to the Cu-MOF, the diffraction angles of BTA-Cu-MOF almost do not change, which suggested that crystalline form of Cu-MOF is not altered after the addition of BTA. However, the intensity of diffraction peaks of BTA-Cu-MOF became successively weaker. The reason preliminaries was that the BTA was loaded into Cu-MOF [10].

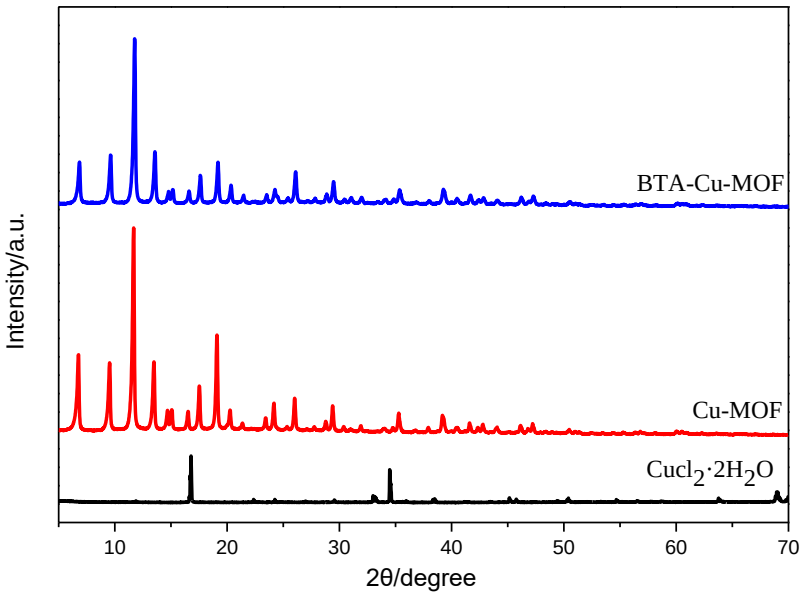

Figure 2. X-ray diffraction spectra of Cu-MOF

3.2. The characterization of BTA-Cu-MOF

In aggressive media, a uniform release rate of the inhibitor (BTA) provides a longer anticorrosion period of functional coatings. To better understand and assess the release process of BTA from the containers, UV-vis spectroscopy was employed to observe the variation in the release rate by means of absorbance. The concentration-absorbance curve of BTA (different concentration BTA/EtOH) was used as a standard to observe the concentration of BTA in BTA-Cu-MOF. The concentration-absorbance standard curve, the fitting curve and fitting equation of BTA are shown in Fig. 3a. The absorbance of BTA in BTA-Cu-MOF was converted into concentration via the fitting equation of the BTA standard curve (fig. 3a). As shown in Fig. 3b, the fitted time-concentration curve of BTA from BTA-Cu-MOF shows that the release rate of BTA is 1.05×10^{-4} g/h, which vividly illustrates that the BTA is uniformly released from the Cu-MOF.

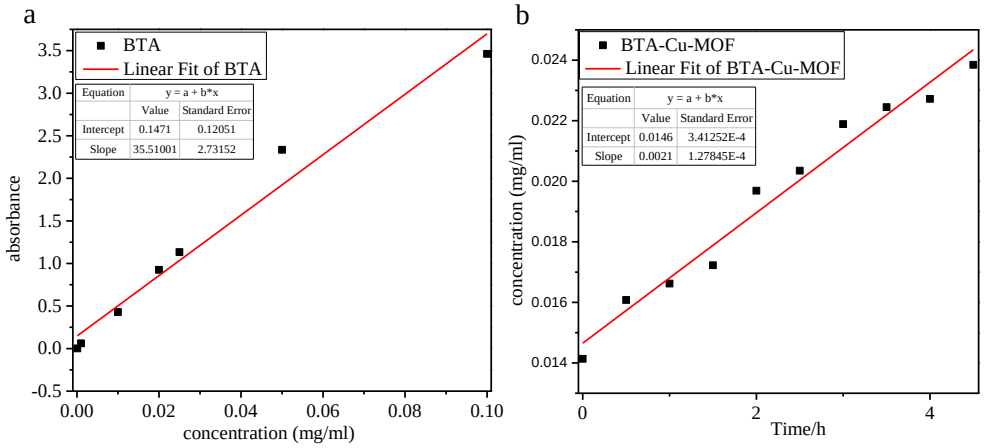

Figure 3. UV-vis spectra of (a) BTA and (b) of BTA-Cu-MOF in ethanol solutions

SEM images of Cu-MOF and BTA-Cu-MOF are showed in Fig. 4. As shown in Fig. 4a, Cu-MOF shows a macro-porous foam-like morphology with closed cell structure. It possesses different size and shape of cells and macro-pores in foams, interconnected with each other. The average pore diameter of the cell was approximately 100 nm[34]. The surface of BTA-Cu-MOF (Fig. 4b) shows similar cell structure with Cu-MOF and more tightness interconnected cell structure, indicating that the BTA was successfully loaded in the Cu-MOF. This also was consistent with XRD and UV-vis. Particularly, EDS data of BTA-Cu-MOF (Fig. 4c) shows that the sample contains 4.69% of N element. Thus, the weight percentage of BTA in BTA-Cu-MOF was about 13.3%.

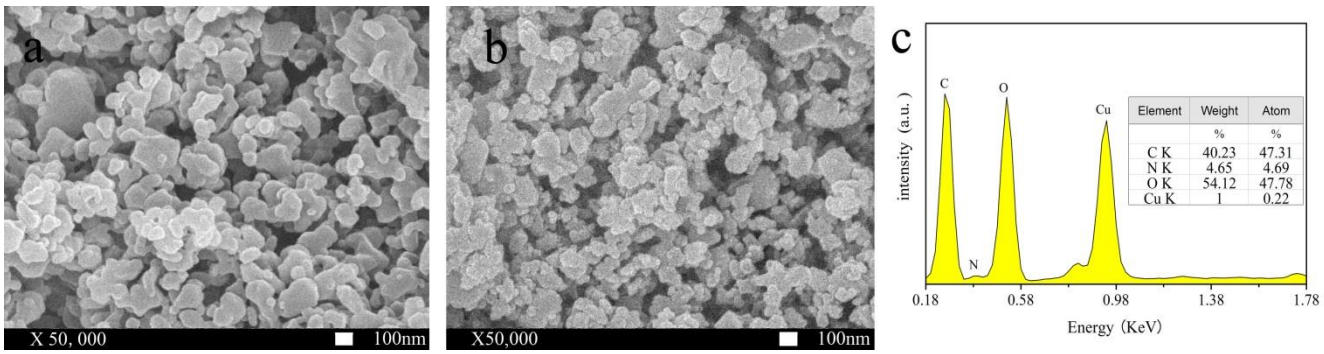

Figure 4. the SEM images of the Cu-MOF (a) and BTA-Cu-MOF (b), and EDS image of BTA-Cu-MOF (c)

Figure 5a provides the thermo gravimetric analysis (TGA) curves of Cu-MOF and BTA-Cu-MOF. There are three major weight losses out of the two samples. The initial weight loss happens between 50-130°C (corresponding to a weight loss of 23.71%) and 50-160°C (6.25%) for Cu-MOF and BTA-Cu-MOF, respectively. This was ascribed to the release of trapped water from Cu-MOF. As for Cu-MOF, the second weight losses happen at 130-280°C (2.83%), which was due to removal of the coordinated water molecule. Meanwhile, weight losses of BTA-Cu-MOF founds at 160-300°C

(15.92%) owing to the decomposition of BTA[10] and removal of the coordinated water molecule. DTG curves of Cu-MOF and BTA-Cu-MOF were shown in Fig. 5b. DTG temperature of Cu-MOF was corresponding to 96°C and 345°C, and DTG temperature of BTA-Cu-MOF was 265°C and 345°C, which was due to the BTA to displace water from Cu-MOF. Thus, the weight percentage of BTA in BTA-Cu-MOF was about 13.09%. Decomposition of the framework ligand of Cu-MOF and BTA-Cu-MOF was respectively at 280-380°C (29.5%) [34] and 300-400°C (31.4%). Thus, Cu-MOF was prepared and BTA was loaded in the Cu-MOF, successfully.

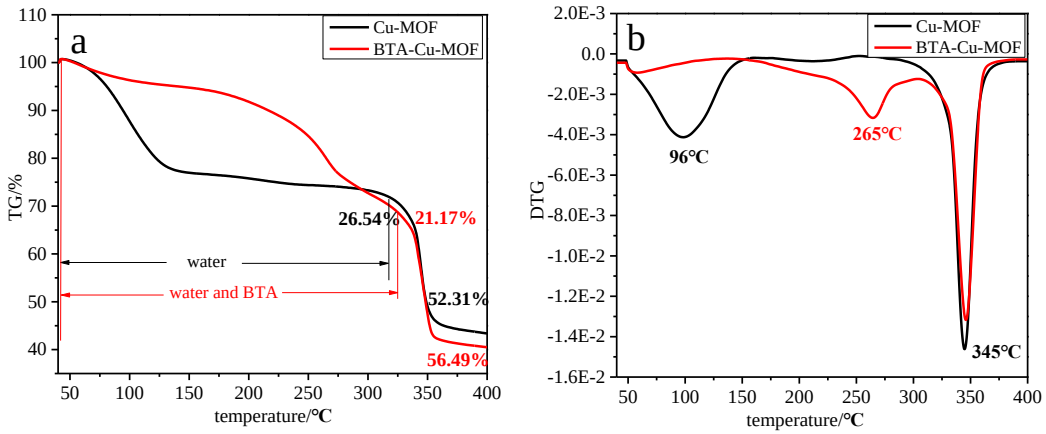

Figure 5. The TGA (a) and DTG (b) curves of Cu-MOF and BTA-Cu-MOF

3.3. Dispersity of BTA-Cu-MOF in the epoxy coating

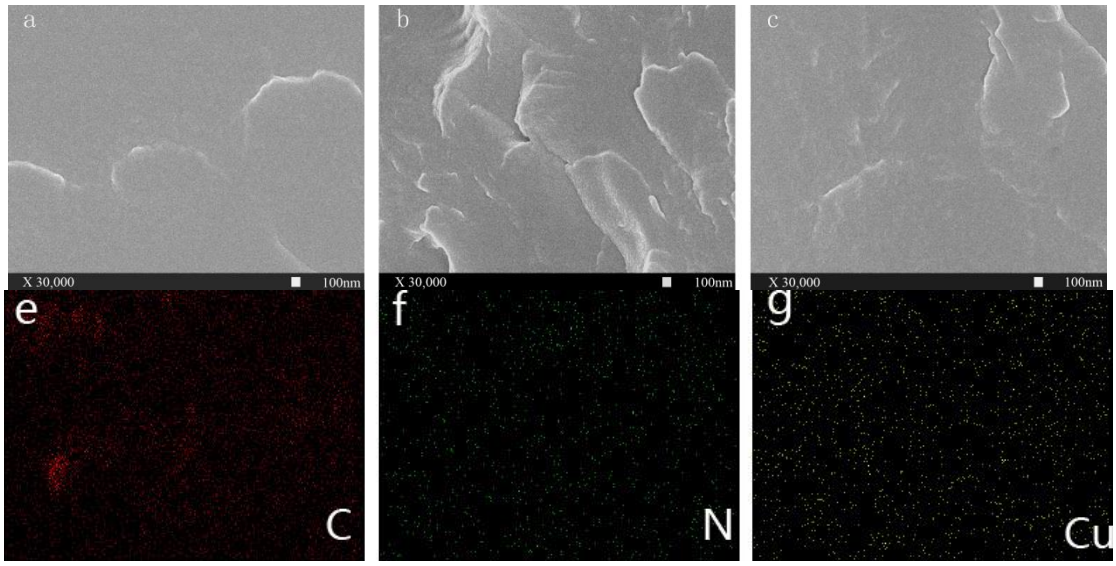

Figure 6. The SEM graphs of fracture surfaces of EP, Cu-MOF/EP and BTA-Cu-MOF/EP (a, b and c), and C, Cu and N mapping (e, g and f) of BTA-Cu-MOF/EP

The images from SEM images of the fractured surfaces of the pure EP, Cu-MOF/EP and BTA-Cu-MOF/EP, respectively, are shown in Fig. 6a, b and c. A smooth and neat morphology was observed

in the surface of pure EP (Fig. 6a). The fractured morphology of the Cu-MOF/EP showed large-scale wrinkle (Fig. 6b), which implied that Cu-MOF was dispersed in EP matrix.

In contrast to the Cu-MOF/EP, the polymer containing BTA-Cu-MOF showed less wrinkle fractured morphology, as showed in Fig. 6c. Also, the fractured image and corresponding N, Cu and C mapping analysis of BTA-Cu-MOF/EP were shown in Fig. 6e-f. Cu (Fig. 6g) and C (Fig. 6e) element were uniformly distributed in the EP matrix, and they were the primary chemical element of MOF that was synthesized though the coordination reaction between Cu and trimesic acid. Meanwhile, the N element (Fig. 6f) was also uniformly distributed in the EP matrix and it did only exist in the BTA. Therefore, these results could provide additional support for the distribution of BTA-Cu-MOF within EP matrix.

The XRD pattern (Fig. 7) of pure epoxy coating, BTA-Cu-MOF/EP coating (blue solid) and BTA-Cu-MOF material (blue powder) was used for research the dispersion of BTA-Cu-MOF material in the epoxy coating. For the pure epoxy coating, a wide diffraction range from 10° to 30° stemmed from the amorphous structure of the cured epoxy molecules[35-37]. Additionally, BTA-Cu-MOF/EP coating showed the similar diffraction patterns as the neat epoxy. And diffraction peaks of BTA-Cu-MOF material disappeared. Therefore, the BTA-Cu-MOF material had the excellent dispersion in EP matrix to some extent. We could infer that the corrosion protection property of BTA-Cu-MOF/EP coating was unexceptionable than pure epoxy coating.

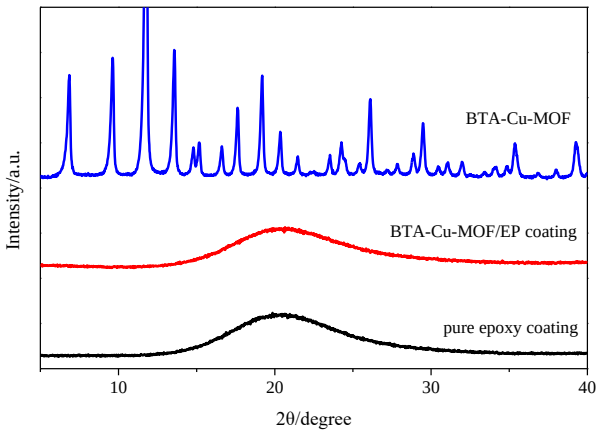

Figure 7. The XRD spectra of pure epoxy coating, BTA-Cu-MOF/EP coating and BTA-Cu-MOF/EP material

3.4. Corrosion resistance of BTA-Cu-MOF in the epoxy coating

The electrochemical impedance spectroscopy (EIS) was employed to characterize corrosion protective performance of the coating with inhibitor-loaded BTA-Cu-MOF in 3.5 wt% NaCl solution. Fig. 9 was Nyquist diagram of pure epoxy, Cu-MOF/EP, 1 wt% BTA-Cu-MOF/EP, 2 wt% BTA-Cu-MOF/EP, 3 wt% BTA-Cu-MOF/EP and 5 wt% BTA-Cu-MOF/EP coatings after 2 h. And the corrosion process of coating was consistent with the Nyquist impedance of the sample [38, 39]. Therefore, the bigger radius of impedance arc is, the more excellent corrosion protective performance

of the coating is. And the equivalent electric circuit (Fig. 8) was modeled by impedance data using a simple electrical equivalent circuit (R(RQ(RQ)) and the fitting results were presented in Table 1. In the equivalent electric circuit, the constant phase element *R*s, *C*c, *R*c, *R*ct and CPEdl denoted the electrolyte resistance, coating capacitance, coating resistance, charge transfer resistance and double layer capacitance, respectively. The coating resistance Rc and charge transfer resistance Rct are two important parameters to evaluate the protective performance for metals. The coating resistance Rc can reflect the defects and degradation degree of coatings. With the degradation of the coating, more defects will form and will result in the lower value of coating resistance. In addition, the charge transfer resistance (Rct) directly relates to the rate of the corrosion process at the electrolyte/metal interface [40, 41]. The higher the Rct is, the lower the corrosion rate is. The radius of impedance arc of all coating decreased in the order of 2 wt% BTA-Cu-MOF/EP > 3 wt% BTA-Cu-MOF/EP > 5 wt% BTA-Cu-MOF/EP > 1 wt% BTA-Cu-MOF/EP > Cu-MOF/EP > pure epoxy. And 2 wt% BTA-Cu-MOF/EP had higher coating resistance and charge transfer resistance than that of other coatings. Thus, compared with pure epoxy and Cu-MOF/EP, corrosion protection performance of BTA-Cu-MOF/EP coating exhibited a significant increase coating owing to that BTA was an excellent corrosion inhibitor[42]. And the optimum weight of BTA-Cu-MOF was 2 wt%.

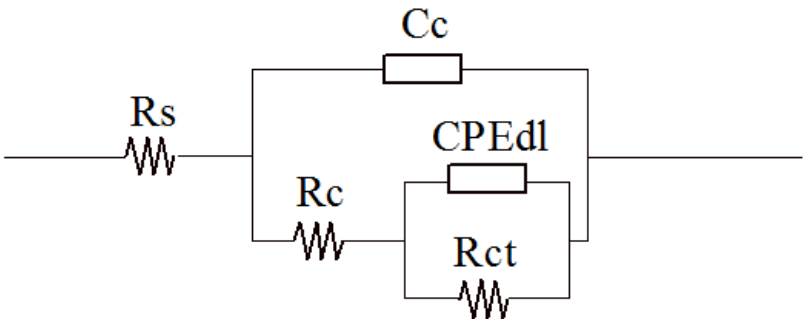

Figure 8. the equivalent electric circuit of coating

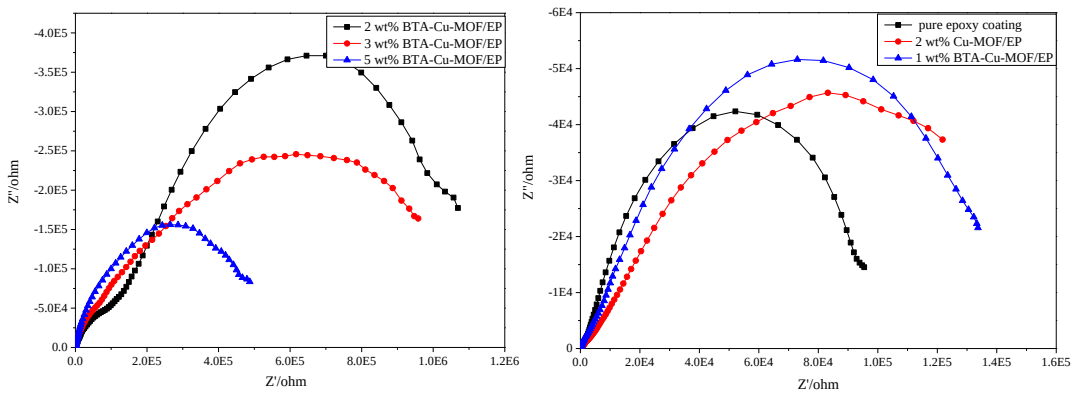

Figure 9. Nyquist plots of all coatings after soaking for 2h

Table 1. Fitting results of the equivalent electrical circuits after 2h immersion

Coating	pure epoxy	2 wt% Cu-MOF/EP	1 wt% BTA-Cu-MOF/EP	2 wt% BTA-Cu-MOF/EP	3 wt% BTA-Cu-MOF/EP	5 wt% BTA-Cu-MOF/EP
Rc (Ω cm^2)	2.252E7	4.871E6	1.726E6	6.789E6	1.217E7	9.134E5
Rct (Ω cm^2)	2.851E6	1584E7	1.896E7	1.418E8	3.551E7	3.553E7

The potentiodynamic polarization test was performed for pure epoxy, Cu-MOF/EP and BTA-Cu-MOF/EP coatings after 2h immersion in a 3.5 wt% aqueous NaCl solution. Potentiodynamic polarization curves of all cases is shown in Fig. 10. The corrosion potential for Cu-MOF/EP and BTA-Cu-MOF/EP coatings are more positive than that observed in the case of pure epoxy. The corrosion current density, Icorr, values for BTA-Cu-MOF/EP coatings to decrease gradually as the amounts of BTA-Cu-MOF increase up to 2 wt%. Thus, 2 wt% BTA-Cu-MOF/EP coating has the lowest value of Icorr (5.86E-7 A/cm^2). On the other hand, the most positive value for Ecorr (-0.3123 V versus SCE) indicates that 2 wt% BTA-Cu-MOF/EP samples have thermodynamically the lowest corrosion tendency after 2h immersion.

The polarization resistance (Rp) was evaluated from the potentiodynamic polarization curves according to Stern–Geary equation [2]:

$$Rp = \frac{\beta_a * \beta_c}{2.303 * I_{corr}(\beta_a + \beta_c)} \quad (1)$$

Where Icorr, β_a and β_c are the corrosion current density, anodic potentiodynamic polarization slope and cathodic potentiodynamic polarization slope, respectively. The steel coated with neat epoxy has the greatest negative Ecorr value in comparison to Cu-MOF/EP and BTA-Cu-MOF/EP samples.

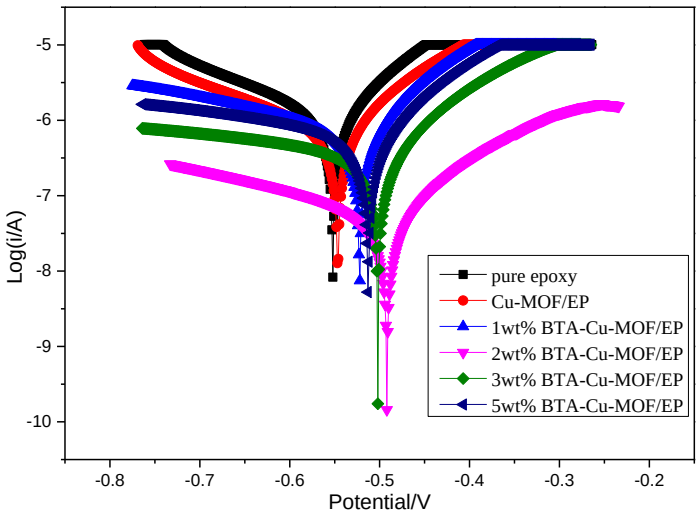

Figure 10. Potentiodynamic polarization curves was measured after 2h immersion

Table 2. Electrochemical parameters obtained from potentiodynamic polarization measurements after 2h immersion of samples.

sample	Ecorr V/SCE	Icorr($A \cdot cm^{-2}$)	RpΩ/cm^2
pure epoxy	0.5518	1.339E-6	22512.3
Cu-MOF/EP	0.5471	8.356E-7	37256.5
1wt%BTA-Cu-MOF/EP	0.5224	7.604E-7	41677.6
2wt%BTA-Cu-MOF/EP	0.4919	6.491E-8	595543.9
3wt%BTA-Cu-MOF/EP	0.5022	4.299E-7	98359.5
5wt%BTA-Cu-MOF/EP	0.5131	7.229E-7	55084.9

For example, 2 wt% BTA-Cu-MOF/EP samples exhibited a corrosion potential of 0.4919 V versus SCE which implies polarization resistance (Rp) value of 0.5955 $M\Omega/cm^2$ in 3.5 wt% NaCl electrolyte which is 26.4 time the Rp of neat epoxy. The electrochemical parameters (anodic potentiodynamic polarization slope (β_a), cathodic potentiodynamic polarization slope (β_c), Icorr, Ecorr, Rp and Rcorr) are summarized in Table 2.

Water permeability of coating was measured to determine the corrosion prevention of coating owing to the corrosive medium through the micropores resulting from the contact between the substrate and the corrosive environment [43, 7]. And water contact angles (WCAs) and typical images of water droplets on pure epoxy, Cu-MOF/EP, 1wt% BTA-Cu-MOF/EP, 2wt% BTA-Cu-MOF/EP, 3wt% BTA-Cu-MOF/EP and 5wt% BTA-Cu-MOF/EP coating were shown in Fig. 11. Before immersion, the contact angles of above all coatings respectively was 80.3, 88.18, 90.62, 99.79, 93.79 and 92.49. After immersion, these contact angles respectively were altered to 70.8, 78.5, 80.1, 91.3, 86.1 and 83.5. Therefore, pure epoxy coating presented hydrophilic properties. And the WCAs of Cu-MOF/EP and BTA-Cu-MOF/EP showed increasing phenomena. Interestingly, BTA-Cu-MOF/EP coating wholly exhibited the hydrophobicity. It was noted that the lower hydrophilic surface could notably extend the preliminary soaking stage owing to lower hydrophilic increase the wettability time of coatings' surface to protect the steel [44, 45]. After 7 days of immersion, the WCAs of all coating decreased obviously which revealed that the anticorrosion performance of epoxy coatings was degraded slightly with the extension of immersion time. Remarkably, the WCA of 2wt% BTA-Cu-MOF/EP still remained at a maximum and exhibited the hydrophobicity, reflecting surface of the sample reduced the contacting with the corrosive medium to prevent steel from corrosion in a relatively long time compared to other epoxy coatings. Namely, 2wt% BTA-Cu-MOF/EP coating had a more outstanding anticorrosion performance and more prolonged anti-corrosion time.

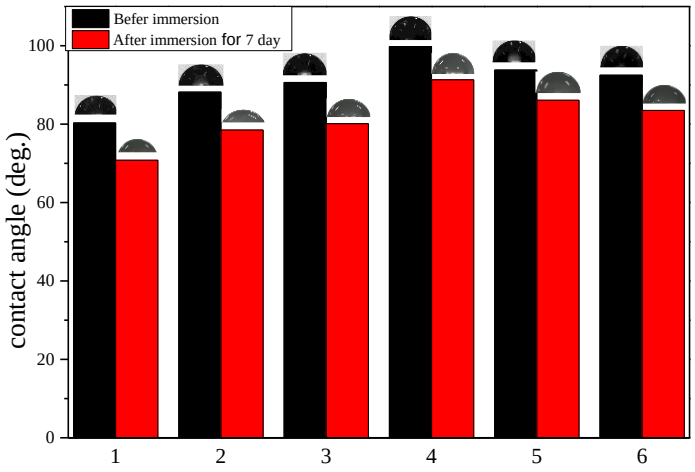

Figure 11. The water contact angles and typical images of water droplets on the pure epoxy coating (1), Cu-MOF/EP coating (2), 1wt% BTA-Cu-MOF/EP coating (3), 2wt% BTA-Cu-MOF/EP coating (4), 3wt% BTA-Cu-MOF/EP coating (5) and 5wt% BTA-Cu-MOF/EP coating(6)

4. CONCLUSIONS

In conclusion, Cu-MOF was synthesized by coordination reaction between $Cucl_2 \cdot 2H_2O$ and trimesic acid and then loading BTA into the Cu-MOF, and the material was characterized by FT-IR, SEM, and XRD. The BTA-Cu-MOF was well dispersed in epoxy resin. The effect of BTA-Cu-MOF concentration on anti-corrosion properties of epoxy coating has been studied by EIS and water contact angle. EIS measurements indicated the anti-corrosion properties of all coating decreased in the order of 2 wt% BTA-Cu-MOF/EP coating > 3 wt% BTA-Cu-MOF/EP coating > 5 wt% BTA-Cu-MOF/EP coating > 1 wt% BTA-Cu-MOF/EP coating > Cu-MOF/EP coating > pure epoxy coating. Water penetration of 2 wt% BTA-Cu-MOF/EP coatings was also worst of all coatings. Therefore, the coating containing 2 wt% BTA-Cu-MOF particles exhibit best corrosion prevention properties than other coatings.

ACKNOWLEDGEMENT
This work was supported by Open Fund (TLN201617) of State Key Laboratory of Oil and Gas Reservoir Geology and Exploitation(Southwest Petroleum University), and Southwest Petroleum University petroleum pipe service safety youth science and technology innovation team (No. 2018CXTD01)

References

1. F. Tang, G. Chen, R.K. Brow, J.S. Volz, M.L. Koenigstein, *Corros. Sci.*, 59 (2012) 157.
2. S. Pour-Ali, C. Dehghanian, A. Kosari, *Corros. Sci.*, 90 (2015) 239.
3. S. Bera, T.K. Rout, G. Udayabhanu, R. Narayan, *Prog. Org. Coat.*, 101 (2016) 24.
4. S. Niroumandrad, M. Rostami, B. Ramezanzadeh, *Prog. Org. Coat.*, 101 (2016) 486.
5. Z. Yu, L. Lv, Y. Ma, H. Di, Y. He, *RSC. Adv.*, 6 (2016) 18217.
6. M. Bahrami, Z. Ranjbar, R.A. Khosroshahi, S. Ashhari, *Prog. Org. Coat.*, 113 (2017) 25.

7. M.A. Deyab, R. Ouarsal, A.M. Al-Sabagh, M. Lachkar, B.E. Bali, *Prog. Org. Coat.*, 107 (2017) 37.
8. V.P. Poornima, A. Tanvir, Y.H. El-Gawady, M.A.A. Alma'Adeed, *Prog. Org. Coat.*, 112 (2017) 127.
9. L. Huang, N. Yi, Y. Wu, Y. Zhang, Q. Zhang, Y. Huang, Y. Ma, Y. Chen, *Adv. Mater.*, 25 (2013) 2224.
10. Y. He, W. Xu, R. Tang, C. Zhang, Q. Yang, *Rsc. Adv.*, 5 (2015) 90609.
11. H. Di, Z. Yu, Y. Ma, Y. Pan, H. Shi, L. Lv, F. Li, C. Wang, T. Long, Y. He, *Polym. Advan. Technol.*, 27 (2016) 915.
12. S.H. Sonawane, B.A. Bhanvase, A.A. Jamali, S.K. Dubey, S.S. Kale, D.V. Pinjari, R.D. Kulkarni, P.R. Gogate, A.B. Pandit, *Chem. Eng. J.*, s 189–190 (2012) 464.
13. Y.H. Lei, N. Sheng, A. Hyono, M. Ueda, T. Ohtsuka, *Prog. Org. Coat.*, 77 (2014) 339.
14. Y. Qiang, S. Zhang, S. Xu, W. Li, *J. Colloid. Interf. Sci.*, 472 (2016) 52.
15. D.G. Shchukin, H. Moehwald, *J. Cheminform.*, 47 (2011) 8730.
16. M.L. Zheludkevich, J. Tedim, M.G.S. Ferreira, *Electrochimica. Acta.*, 82 (2012) 314.
17. H.K. Singh, K.V. Yeole, S.T. Mhaske, *Chem. Eng. J.*, 295 (2016) 414.
18. X. Li, I. Nikiforow, K. Pohl, J.r. Adams, D. Johannsmann, *Coatings.*, 3 (2013) 16.
19. D. Grigoriev, D. Akcakayiran, M. Schenderlein, D. Shchukin, *Corrosion.*, 70 (2014) 446.
20. M.F. Montemor, *Surf. Coat. Technol.*, 258 (2014) 17.
21. X.Z. Gao, H.J. Liu, F. Cheng, Y. Chen, *Chem. Eng. J.*, 283 (2016) 682.
22. D.A. Leal, I.C. Riegel-Vidotti, M.G.S. Ferreira, C.E.B. Marino, *Corros. Sci.*, (2017).
23. M. Sun, A. Yerokhin, M.Y. Bychkova, D.V. Shtansky, E.A. Levashov, A. Matthews, *Corros. Sci.*, 111 (2016) 753.
24. K.M. Choi, J.H. Park, J.K. Kang, *Chem. Mater.*, 27 (2015) 5088.
25. T.C. Wang, W. Bury, D.A. Gomezgualdron, N.A. Vermeulen, J.E. Mondloch, P. Deria, K. Zhang, P.Z. Moghadam, A.A. Sarjeant, R.Q. Snurr, *J. Am. Chem. Soc.*, 137 (2015) 3585.
26. J. An, S.J. Geib, N.L. Rosi, *J. Am. Chem. Soc.*, 131 (2009) 8376.
27. M. Jahan, Q. Bao, J.X. Yang, K.P. Loh, *J. Am. Chem. Soc.*, 132 (2010) 14487.
28. D. Cunha, M.B. Yahia, S. Hall, S.R. Miller, H. Chevreau, E. Elkaïm, G. Maurin, P. Horcajada, C. Serre, *Chem. Mater.s*, 25 (2013) 2767.
29. Q. Hu, J. Yu, M. Liu, A. Liu, Z. Dou, Y. Yang, *J. Med. Chem.*, 57 (2014) 5679.
30. E.D.H. Etaiw, E.A.S. Fouda, S.A. Amer, M.M. El-Bendary, *J. Inorg. Organomet. P.,* 21 (2011) 327.
31. Y. Fang, X. Li, F. Li, X. Lin, M. Tian, X. Long, X. An, Y. Fu, J. Jin, J. Ma, *J. Power. Sources.*, 326 (2016) 50.
32. E.A.S. Fouda, E.D.H. Etaiw, M.M. El-Bendary, M.M. Maher, *J. Mol. Liq.*, 213 (2016) 228.
33. N. Wang, Y. Zhang, J. Chen, J. Zhang, Q. Fang, *Prog. Org. Coat.*, 109 (2017) 126.
34. S. Kumaraguru, R. Pavulraj, S. Mohan, *T. I. Met. Finish.*, 95 (2017).
35. L.Z. Guan, Y.J. Wan, L.X. Gong, D. Yan, L.C. Tang, L.B. Wu, J.X. Jiang, G.Q. Lai, *J. Mater. Chem. A.*, 2 (2014) 15058.
36. Y.J. Wan, L.X. Gong, L.C. Tang, L.B. Wu, J.X. Jiang, *Compos. Part. A.*, 64 (2014) 79.
37. Z. Yu, H. Di, Y. Ma, Y. He, L. Liang, L. Lv, X. Ran, Y. Pan, Z. Luo, *Surf. Coat. Technol.*, 276 (2015) 471.
38. M. Nematollahi, M. Heidarian, M. Peikari, S.M. Kassiriha, N. Arianpouya, M. Esmaeilpour, *Corros. Sci.*, 52 (2010) 1809.
39. C. Chen, S. Qiu, M. Cui, S. Qin, G. Yan, H. Zhao, L. Wang, Q. Xue, *Carbon.*, 114 (2017) 356.
40. N. Parhizkar, T. Shahrabi, B. Ramezanzadeh, *Corros. Sci.*, 123 (2017) 55.
41. X. Quan, J. Wang, S. Zhao, W. Cai, Z. Wang, S. Wang, X. Cui, *Prog. Org. Coat.*, 115 (2018) 9.
42. Y. Feng, Y.F. Cheng, *Chem. Eng. J.*, 315 (2017) 537.
43. Y. Ma, H. Di, Z. Yu, L. Liang, L. Lv, Y. Pan, Y. Zhang, D. Yin, *Appl. Surf. Sci.*, 360 (2016) 936.

44. S. Shreepathi, S.M. Naik, M.R. Vattipalli, *J. Coat. Technol. Res.*, 9 (2012) 411.
45. K.C. Chang, M.H. Hsu, H.I. Lu, M.C. Lai, P.J. Liu, C.H. Hsu, W.F. Ji, T.L. Chuang, Y. Wei, J.M. Yeh, *Carbon.*, 66 (2014) 144.